# 18 year record of circum-Antarctic landfast sea ice distribution allows detailed baseline characterisation, reveals trends and variability

Alexander D. Fraser[1], Robert A. Massom[2,1], Mark S. Handcock[3], Phillip Reid[4,1], Kay I. Ohshima[5], Marilyn N. Raphael[6], Jessica Cartwright[7], Andrew R. Klekociuk[2,1], Zhaohui Wang[8], and Richard Porter-Smith[1]

[1]Australian Antarctic Program Partnership, Institute for Marine and Antarctic Studies, University of Tasmania, Hobart, Tasmania 7001, Australia
[2]Australian Antarctic Division, Channel Highway, Kingston, Tasmania 7050, Australia
[3]Department of Geography, University of California, Los Angeles, CA 90095, USA
[4]Bureau of Meteorology, 111 Macquarie St, Hobart, Tasmania 7000, Australia
[5]Institute of Low Temperature Science, Hokkaido University, Sapporo 060-0819, Japan
[6]Department of Statistics, University of California, Los Angeles, CA 90095, USA
[7]Spire Global, Inc., Glasgow, G3 8JU, UK
[8]Institute for Marine and Antarctic Studies, University of Tasmania, Hobart, Tasmania 7001, Australia

**Correspondence:** Alexander D. Fraser (Alexander.Fraser@utas.edu.au)

**Abstract.** Landfast sea ice (fast ice) is an important though poorly-understood component of the cryosphere on the Antarctic continental shelf, where it plays a key role in atmosphere-ocean-ice sheet interaction and coupled ecological and biogeochemical processes. Here, we present a first in-depth baseline analysis of variability and change in circum-Antarctic fast-ice distribution (including its relationship to bathymetry), based on a new high-resolution satellite-derived time series for the period 2000 to 2018. This reveals a) an overall trend of -882 ± 824 km$^2$/y (-0.19 ±0.18 %/y); and b) eight distinct regions in terms of fast-ice coverage and modes of formation. Of these, four exhibit positive trends over the 18 y period and four negative. Positive trends are seen in East Antarctica and in the Bellingshausen sea, with this region claiming the largest positive trend of +1,198 ± 359 km$^2$/y (+1.10 ± 0.35 %/y). The four negative trends predominantly occur in West Antarctica, with the largest negative trend of -1,206 ± 277 km$^2$/y (-1.78 ± 0.41 %/y) occurring in the Victoria and Oates Lands region in the eastern Ross Sea. All trends are significant. This new baseline analysis represents a significant advance in our knowledge of the current state of both the global cryosphere and the complex Antarctic coastal system that is vulnerable to climate variability and change. It will also inform a wide range of other studies.

## 1 Introduction

Around Antarctica, landfast or fast ice is a stationary and consolidated form of sea ice which is attached to, and held in place by, the coastline or floating ice shelf fronts (World Meteorological Organization, 1970) and icebergs grounded in waters shallower than approximately 400 m (Giles et al., 2008; Fraser et al., 2012). As such, Antarctic fast ice forms only on the continental shelf,

typically in narrow (50 to 250 km wide) bands adjacent to the coast and/or upstream of protrusions into the westward Antarctic Coastal Current that intercept encroaching (drifting) pack ice (Fraser et al., 2012; Nihashi and Ohshima, 2015). Depending on location, Antarctic fast ice can range in persistence from annual through perennial to multi-decadal (e.g., Massom et al.,

20 2010a), with certain regions being highly variable and breaking out and reforming several times per year (e.g., Massom et al., 2009; Fraser et al., 2012).

Antarctic fast ice is not only a sensitive bellwether of climate change and variability, given its intimate linkage and interaction with the high-latitude ocean and atmosphere (Massom et al., 2009; Fraser, 2011; Aoki, 2017). Its distribution also influences the size of adjacent coastal polynyas (Massom et al., 1998, 2001; Nihashi and Ohshima, 2015; Fraser et al., 2019), affecting

25 regional rates of sea-ice production, water mass modification and the formation of globally-important Antarctic Bottom Water in certain key locations (e.g., Kusahara et al., 2017; Ohshima et al., 2013). Moreover, recent work has shown the importance of fast ice in mechanically bonding and stabilising vulnerable outer margins of floating glacier tongues and ice shelves (Massom et al., 2018; Massom et al., 2015; Massom et al., 2010a), and also in controlling the seasonal dynamics and discharge rate of certain outlet glaciers (Greene et al., 2018). Fast ice is also of major ecological importance as a key breeding habitat for

30 emperor penguins and Weddell seals (Kooyman and Burns, 1999; Massom et al., 2009), plays a role in structuring shallow coastal benthic ecosystems (Clark et al., 2017) and is a region of high primary productivity (concentrated ice algal growth (Meiners et al., 2018)). Coastal fast ice also constitutes a reservoir of nutrients (de Jong et al., 2013) which can substantially enhance primary production in the coastal zone when released into the water column upon fast-ice breakout/melt (particularly for thick, multi-year fast ice, e.g., Shadwick et al., 2013). Finally, fast ice can either facilitate or impede aviation and station

35 resupply activities, depending on its location, extent and thickness (The Council of Managers of National Antarctic Programs (COMNAP), 2015). It follows that change and/or variability in Antarctic fast-ice distribution and seasonality have wide-ranging ramifications, and characterisation of where and how fast ice is changing is a high priority.

Accurate, consistent, long-term and year-round time-series mapping of Antarctic fast ice at a high spatio-temporal resolution and on a circumpolar scale requires satellite observation, but is technically challenging (Fraser et al., 2009, 2010; Nihashi and

40 Ohshima, 2015; Fraser et al., 2020; Kim et al., 2018; Kim et al., 2020; Li et al., 2020). Knowledge of its distribution and trends has been identified as a major gap (Vaughan et al., 2013; Meredith et al., 2019). This has severely limited our understanding of the important coastal icescape and key interactive physical, biological and biogeochemical processes therein. Fraser et al. (2012) released an 8.8 y dataset of East Antarctic fast ice extent from 2000 to 2008, but this dataset has not been updated. Using passive microwave satellite data, Nihashi and Ohshima (2015) subsequently produced a dataset of circum-Antarctic fast

45 ice extent from 2003 to 2011, but at a relatively coarse resolution of 6.25 km/pixel, and this technique does not detect and include young fast ice (Fraser et al., 2019). Li et al. (2020) recently released a high spatial resolution circum-Antarctic dataset of fast ice covering November only in the years 2006-11 and 2016-17 using synthetic aperture radar (SAR) image analysis. However, since November is a month characterised by regionally-variable fast ice retreat (Fraser et al., 2012), it is inadequate for analysis of long term trends in extent.

50 As such, detailed circumpolar characterisation of fast ice has not been possible due to the lack of suitable underlying dataset. This gap has recently been filled by the publication of a new time series of fast ice extent from March 2000 to March 2018

(Fraser et al., 2020). This dataset contains 432 contiguous maps of fast ice extent at a 1 km and 15 d resolution, generated by compositing cloud-free visible and thermal infrared imagery from NASA Moderate Resolution Imaging Spectroradiometer (MODIS) sensors onboard the Terra and Aqua satellites (Fraser et al., 2009, 2010).

55     Here, we use this newly-released dataset to perform a first detailed characterisation of circum-Antarctic fast ice distribution, change and variability. We first identify eight distinct regions in terms of fast ice co-variability, which form the basis of the new analysis of fast ice trends around Antarctica. These regions differ from those more traditionally used in Antarctic sea ice analyses (Zwally et al., 1983). We then present the overall extent time series and annual climatology, spatial characterisation of mean fast ice persistence, age and timing of minimum/maximum extent across the 18 y dataset. We also analyse fast ice

60 persistence in concert with bathymetric depth, and interpret this regionally, to more widely assess and determine the linkages between fast ice and grounded icebergs, which act both as stable anchor points for fast ice formation (e.g., Massom et al., 2009; Li et al., 2020) and to intercept and retain encroaching pack ice, thus encouraging fast ice formation upstream (Massom et al., 2001; Massom, 2003).

## 2   Datasets and methods

65 15 day temporal resolution fast ice maps were obtained from a recently-published NASA Moderate Resolution Imaging Spectroradiometer (MODIS)-derived 18 y record of Antarctic fast ice extent (Fraser et al., 2020). This dataset consists of 432 contiguous maps of fast ice extent at a 1 km spatial resolution. This dataset is freely available at http://dx.doi.org/doi:10.26179/5d267d1ceb60c. In this dataset, fast ice maps were constructed following a semi-automated method whereby persistent edges over a 15 d period were taken to be the fast ice edge. Manual intervention was required for times and regions where cloud cover persisted

70 throughout the 15 d window. However, semi-automation was achieved, with 58% of fast ice edge pixels able to be automatically retrieved, marking an advance over earlier, more subjective large-scale fast ice maps (e.g., Fraser et al., 2012).

    To underpin definition of new regions of fast ice co-variability, fast ice anomaly time series are produced for each $1/4°$ of longitude by subtracting the observed $1/4°$ total fast ice from its repeating climatological cycle. New fast ice regions are defined by performing a spatial cross-correlation of these $1/4°$ longitude fast ice anomaly time series. Nearby regions exhibiting

75 similar anomaly co-variability are indicated by positive correlation "pockets", and these are grouped manually to define regions. Automated region selection using a decorrelation length scale minimum-based approach to region delineation, as in Raphael and Hobbs Raphael and Hobbs (2014), was unable to be implemented due to extensive coastal regions with no fast ice. The final step of manual regional selection a) allows grouping of fast ice regions across gaps; and b) avoids excessive partitioning of broader regions. This selection of new regions of fast ice co-variability is detailed in Appendices A and B.

80     Fast ice persistence distribution is characterised by calculating the the fraction of the time series which each pixel is covered by fast ice, after Fraser et al. (2012). This "per-pixel" mapping is also exploited to visualise per-pixel a) timing of minimum and maximum fast ice extent, b) fast ice age and c) trends in extent. The per-pixel trend map is constructed by fitting a linear trend to each pixel's 18 y time series of extent, and plotting the slope (trend) for each pixel. The map of timing of minimum/maximum fast ice extent is constructed by fitting a Fourier series with fundamental (yearly) component as well as 2nd to 4th harmonics

85 to the time series of fast ice extent for each pixel. The Fourier parameters are chosen by Levenberg-Marquardt least-squares minimisation (Markwardt, 2009). The resulting timing of minimum/maximum extent is then extracted from the Fourier fit. Here, we prefer to display timing information in this "day of minimum/maximum" format rather than the traditional maps of "day of advance/retreat" used in other sea ice seasonality studies (e.g., Massom et al., 2013) due to the event-based formation and breakout of fast ice, in contrast to the more fine-grained advance/retreat of sea ice. The mean fast ice age map is constructed

90 by calculating the mean time between fast ice formation and subsequent breakout.

We characterise the distribution of fast ice over bathymetry of varying depth by constructing 2D probability distribution functions of International Bathymetric Chart of the Southern Ocean (IBCSO, Arndt et al. (2013))-derived bathymetric depth (50 m bins) vs fast ice persistence (5 % bins). We use this circum-Antarctic bathymetry compilation despite the caveat that all such compilations suffer from a scarcity of data in fast ice-infested waters, owing to a lack of shipboard sonar measurements

95 (Smith et al., in press). We retrieve the modal value for each persistence bin, then compute the persistence-weighted mean of these modal values to characterise modal formation depth on a circumpolar basis, as well as within the new regions defined here.

We also use sea ice concentration from the National Oceanic and Atmospheric Administration/National Snow and Ice Data Center Climate Data Record of Passive Microwave Sea Ice Concentration, Version 3, to compare timing of sectoral fast ice

100 extent to that of overall sea ice. For this timing comparison, we exploit a new technique to model the seasonal cycle of both sea ice and fast ice presented by Handcock and Raphael (2020). This technique, which models each year's annual cycle as an invariant smoothed spline plus a smoothed trend over time, allows daily-resolution calculation of timing statistics even when the input dataset (i.e., the fast ice dataset) has a ~bi-weekly resolution, thus facilitating a robust timing comparison between fast ice and overall sea ice extent.

105 Circumpolar and regional fast ice trends are computed by calculating the sectoral total fast ice extent, computing the climatological cycle, removing the climatological cycle from the observed totals to form the sectoral anomalies, and fitting a linear trend to the anomalies in each sector. Trend confidence is determined by calculating 95% confidence intervals using the t-distribution. In the calculation of trends, pixels experiencing ice shelf retreat or advance during the 18 y period are removed from this calculation to remove the strong trend contributions caused by these processes.

## 3 Results

### 3.1 Climatological patterns

For the analyses in the following sections, we consider only the eight newly-defined regions (as detailed in the Appendices A and B), plus circumpolar total statistics. Fig. 1 shows the total circumpolar extent time series (a) and its climatological annual cycle (b). A strong annual cycle is evident, with a relatively broad maximum ($\sim$ 601,000 km$^2$) occurring throughout

115 late winter/early spring (day-of-year 273; late September on average), and a well-defined minimum in March ($\sim$221,000 km$^2$, day-of-year 71; mid-March). This indicates that fast ice experiences a seasonal approx. threefold increase in extent. As with overall sea ice (Eayrs et al., 2019; Parkinson, 2019), fast ice displays an asymmetrical annual cycle, experiencing on average

~ 7 months of advance and 5 months of retreat. As such, fast ice as a percentage of overall sea ice area (extent) varies between
a maximum of 12.8 % (8.5 %) in early-mid February (coinciding with the overall sea ice minimum in early-mid February)
120   and around 4.0 % (3.2 %) throughout the winter (mid-July to late November). The largest fast ice contribution is from East
Antarctica, with the Western Indian Ocean, Eastern Indian Ocean and Australia regions together contributing over half of all
fast ice in terms of areal coverage despite only covering 119° of longitude (Table 1).
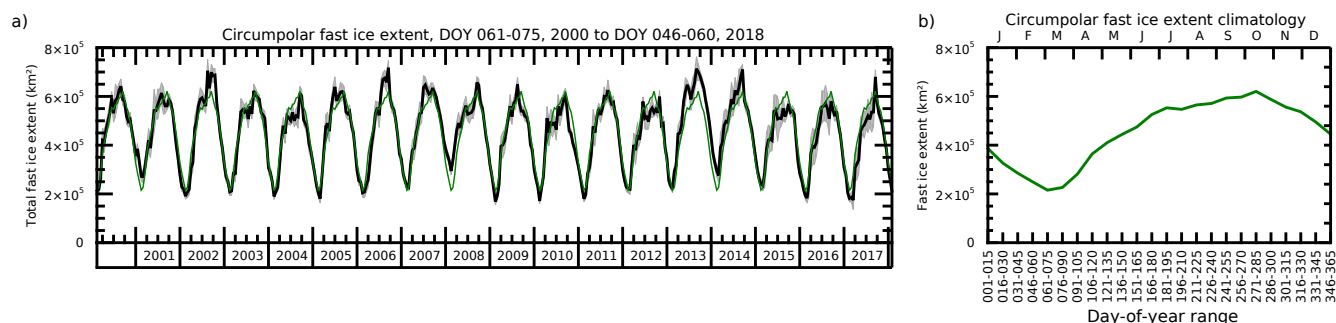
**Figure 1.** a) Bold black line: circumpolar total fast ice extent time series, Mar 2000 - Mar 2018. The gray shading indicates the uncertainty
in the underlying dataset, and the thin green line shows the repeating annual cycle. b) Climatological cycle of total fast ice extent by day of
year.

| Region | Fast ice: Extent ($10^3$ km$^2$) and DOY (brackets) at | | Sea ice: Extent ($10^3$ km$^2$) and DOY (brackets) at | |
| --- | --- | --- | --- | --- |
| | Minimum | Maximum | Minimum | Maximum |
| Circumpolar | 221 (71) | 601 (273) | 3,213 (50) | 18,900 (264) |
| Dronning M. L. (19° W - 18° E) | 4.7(73) | 21 (294) | 99 (51) | 3,122 (269) |
| West Ind. Ocn (27° E - 71° E) | 33 (72) | 111 (264) | 134 (58) | 2,252 (290) |
| East Ind. Ocn (74° E - 103° E) | 24 (74) | 72 (275) | 122 (54) | 1,362 (265) |
| Australia (103° E - 146° E) | 53 (70) | 139 (260) | 173 (53) | 1,112 (275) |
| Vict. Oates L. (146° E - 172° E) | 31 (67) | 85 (285) | 312 (49) | 1,118 (230) |
| Amundsen Sea (102° W - 158° W) | 36 (66) | 66 (246) | 581 (51) | 2,766 (258) |
| Bellings. Sea (60° W - 102° W) | 23 (79) | 64 (275) | 237 (65) | 1,244 (242) |
| Weddell Sea (27° W - 60° W) | 20 (56) | 41 (280) | 1,164 (50) | 2,768 (241) |

**Table 1.** Mean extent (in $10^3$ km$^2$) and mean timing (day-of-year, or DOY) of minimum/maximum extent of both fast ice (left) and overall
sea ice (right) for the entire continent and the eight newly-defined fast ice regions detailed in the Appendix. Dronning M. L. is Dronning
Maud Land, West Ind. Ocn is Western Indian Ocean, East Ind. Ocn is Eastern Indian Ocean, Vict. Oates L. is Victoria and Oates Lands, and
Bellings. Sea is Bellingshausen Sea.

Fig. 2 shows the circumpolar fast ice persistence distribution (as a percentage of average residence time), averaged across
the 18 y dataset. This highlights three broad-scale characteristics: a) widespread regions of intermediate persistence (<∼75%,
125  indicating considerable seasonal growth and decay); b) a zonal width of typically ∼ 50 - 100 km, but up to 250 km (occurring
east of the Mertz Glacier Tongue, ∼145° E); and c) localised regions of near-100% persistence likely corresponding to multi-
year fast ice (which is mapped later in the analysis of fast ice mean age).
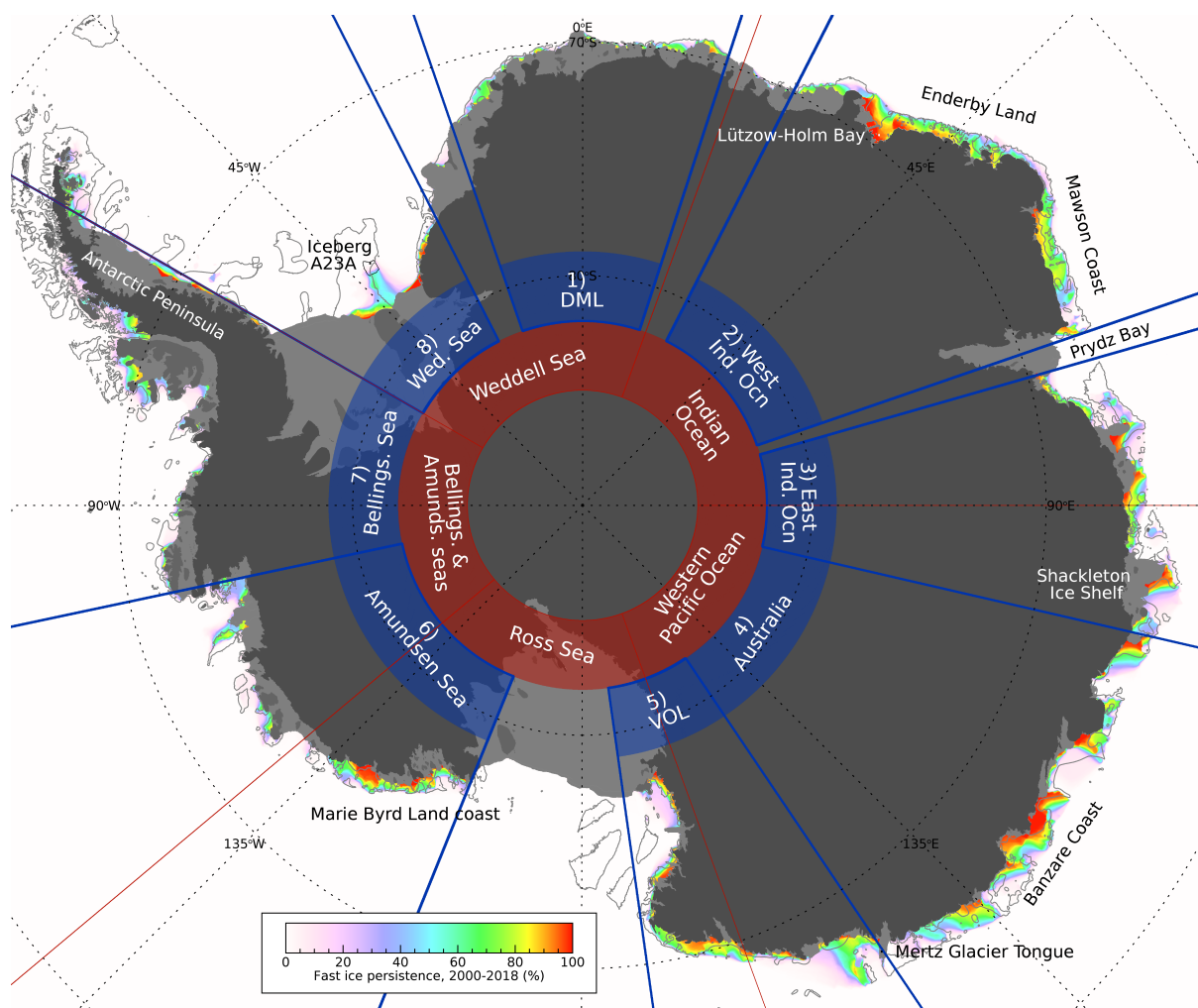
**Figure 2.** Distribution of fast ice persistence, expressed as a percentage of time covering each pixel from Mar 2000 to Mar 2018. Traditional
oceanic sectors are indicated by red boundaries, and newly-defined regions in blue. Gaps between newly-defined regions occur in areas
of minimal fast ice coverage. The 403 m isobath, corresponding to the weighted-mean circumpolar fast ice depth, is indicated as a gray
contour. DML is Dronning Maud Land, VOL is Victoria and Oates Lands. The early-2000 position of large tabular, grounded iceberg A23A
is indicated here in black outline, in the southern Weddell Sea.

Table 1 indicates that both minimum and maximum fast ice extent (day-of-year 71 and 273, respectively) occur later than the corresponding timings for overall sea ice (comprising both pack and fast ice), which are day-of-year 50 (mid-February)

130 and 264 (mid-September), respectively. Regionally, the result of later fast ice minimum is consistent across all regions, however, a later fast ice maximum only occurs in five of eight newly-defined regions (although this may be a consequence of this considerable regional variability in the timing of overall sea ice extent maximum). Maps of timing of minimum and maximum fast ice extent are presented to provide a more localised context for regional studies involving fast ice (Fig. 3). These reveal remarkable differences within neighbouring areas. For example a) Enderby Land fast ice (39° to 52° E) achieves a minimum in

135 April whereas along the Mawson Coast (55° to 71° E) this occurs in February-March; and b) fast ice on the western side of the Antarctic Peninsula reaches minimum later (April) than that on the eastern side (February-March). Regional changes in maximum extent timing are more variable than minimum extent timing, likely due to the broad fast ice peak in the climatological cycle (Fig. 1b). No latitudinal gradient is apparent in either timing metric.

The map of fast ice mean age is presented in Figure 4a. Regions of multi-year fast ice (i.e., mean age >12 months) are

140 typically located either east (upstream) of physical barriers to the westward drift of pack ice in the Antarctic Coastal Current, within deep, sheltered embayments (e.g., Lützow-Holm Bay, ∼40° E), or adjacent to coastal flaw leads indicating the presence of a shear zone (especially in the southern Weddell Sea). As such, the majority is in East Antarctica (e.g., along the Banzare Coast, ∼130° E), although major areas are found throughout the Weddell Sea region and along the Marie Byrd Land coast (∼134 - 159° W). Multi-year ice is generally synonymous with highly-persistent fast ice (i.e., red pixels corresponding to

145 near-100% persistence in Fig. 2), however we find limited regions where relatively low-persistence fast ice (e.g., persisting through 80% of the year on average) can be multi-year (e.g., north of the Wilkins Ice Shelf, ∼74° W), indicating a change to the annual cycle throughout the 18 y study period.

## 3.2 Fast ice extent anomalies and linear trends

The circumpolar total anomaly time series (Fig. 5a) indicates the presence of extended periods with only transient departures

150 from the climatological mean (e.g., 2000 to mid-2007; mid-2008 to 2012), as well as three more persistent departures: extended positive anomalies occurring in mid-2007 to mid-2008; throughout 2013 and 2014; and a negative anomaly from mid-2015 onwards. A marginally-significant (p≃0.04) negative trend of $-882\pm823$ km$^2$/y (-0.19 $\pm$ 0.18 %/y) is reported across Antarctica for the 18 y time series. Under the new region definition, and as shown in Fig. 5b-i, all regions exhibit statistically-significant trends, further indicating that the methodology for defining partitions is robust, even at an inter-decadal time-scale. Four re-

155 gions show positive trends (Dronning Maud Land, Western Indian Ocean, Australia and Bellingshausen Sea regions), with the remainder negative. Strong and opposing trends are frequently observed to occur in adjacent regions indicating that this new partitioning supports preservation of these opposing regional signals.

Per-pixel trends in fast ice extent (Fig. 4b) in excess of $\pm8$ %/y are observed, corresponding to pixels exhibiting an extreme change in fast ice cover across the study period. These occur in areas exhibiting major icescape change, e.g., both upstream

160 and downstream of the Mertz Glacier Tongue (∼144° E), which calved in 2010 Fogwill et al. (2016), and in the Weddell Sea between the Ronne-Filchner Ice Shelf and grounded iceberg A23A, which has gradually drifted northward (Li et al., 2020).
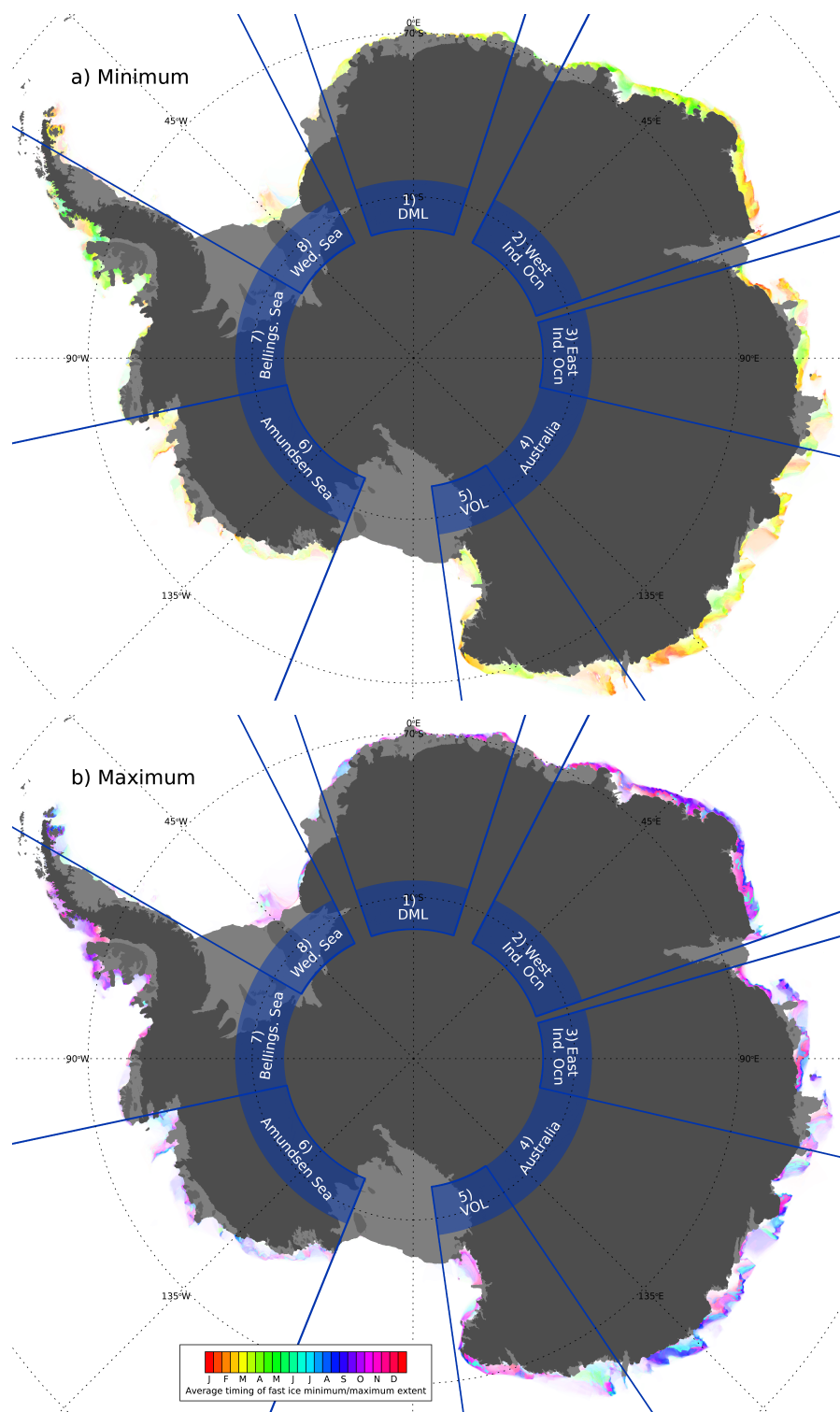
**Figure 3.** Per-pixel average timing of minimum (a) and maximum (b) fast ice extent. For each pixel, color saturation is weighted by annual cycle magnitude (i.e., pixels with persistent multi-year fast ice or no fast ice are transparent.)
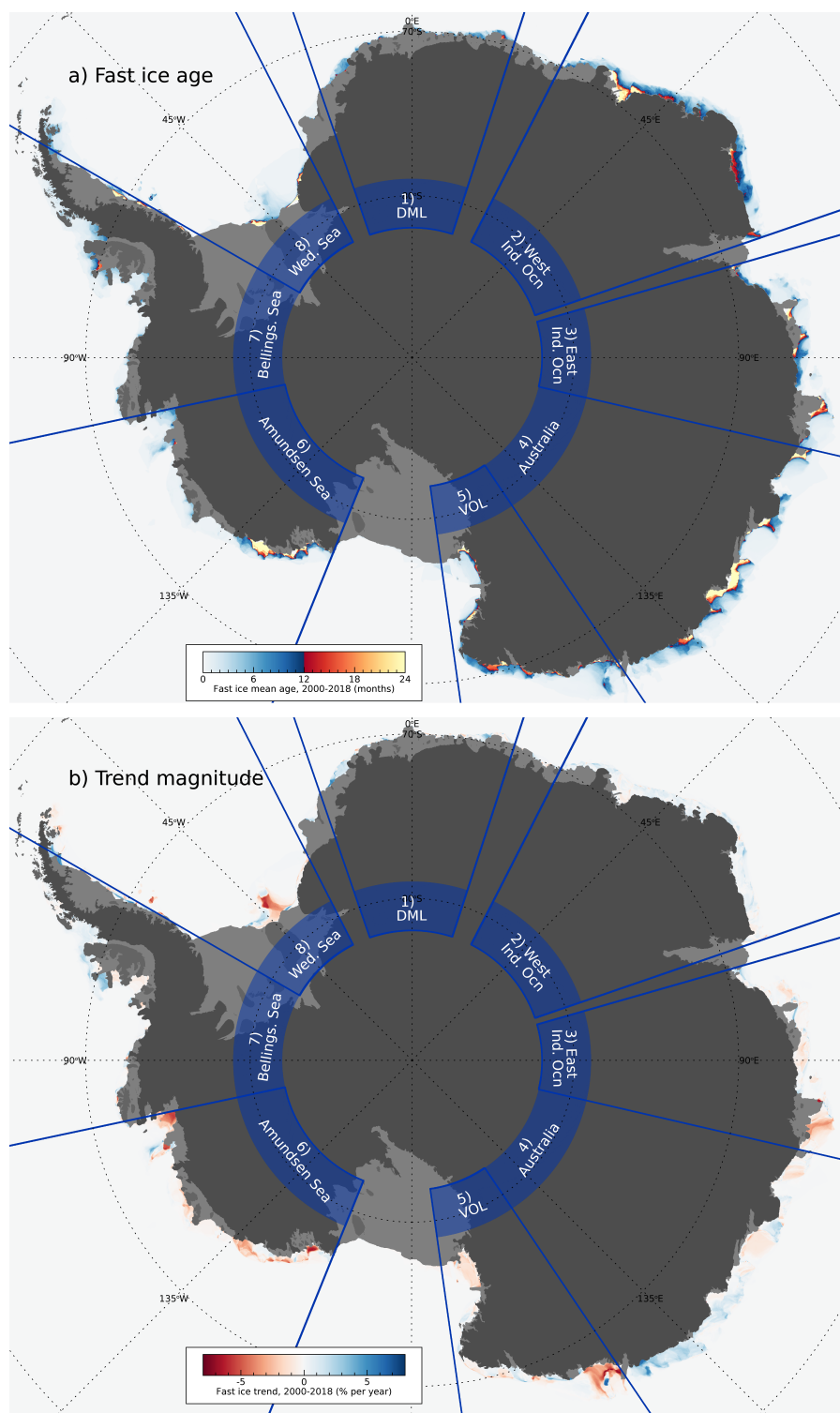
**Figure 4.** a) Mean fast ice age over the 18 y study period. White to blue pixels indicate seasonal fast ice. The color break from a blue hue to a red hue at 12 months is chosen to highlight regions of multi-year fast ice (red-yellow hues). b) Per-pixel trends in fast ice extent (%/y).
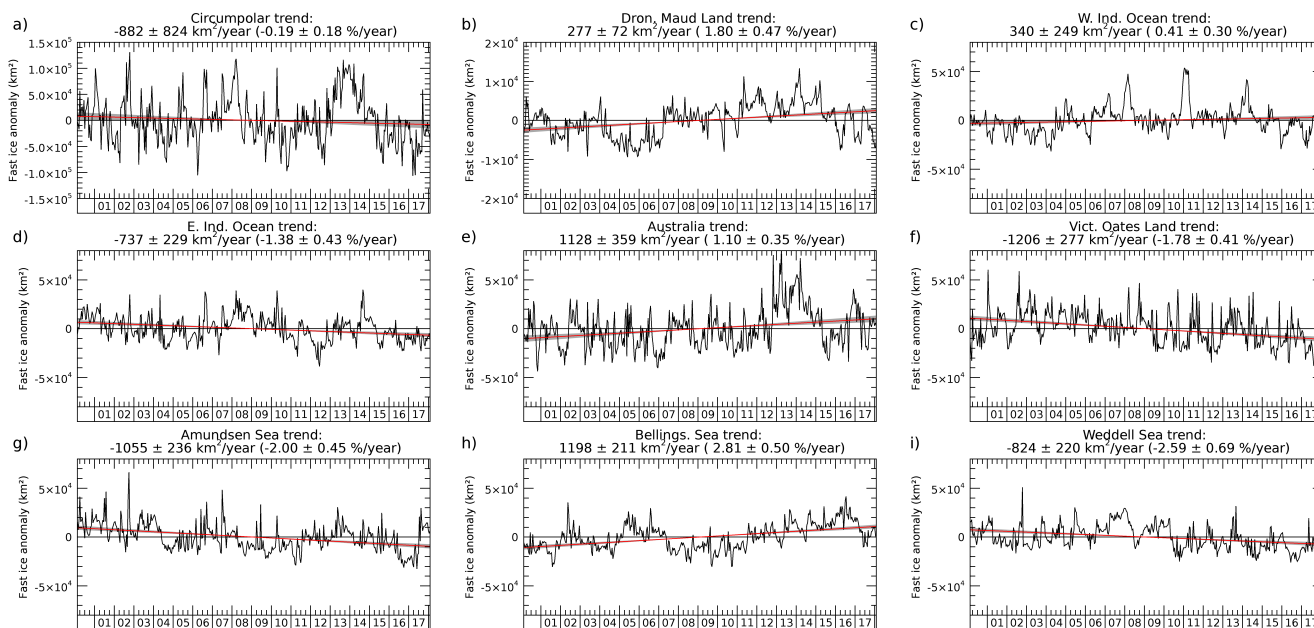
**Figure 5.** Fast ice extent anomalies (black line) and linear trends (red line) for the eight newly-defined fast ice regions. Trend magnitude, bootstrapped 95% confidence interval and trend p-value are indicated in the title of each sub-plot. Note the y-axis scale is the same for all plots except panels a and b. All trends are significant, with a p-value of ≃0.00 for all trends except for the circum-Antarctic (panel a; p≃0.04) and Western Indian Ocean (panel c; p≃0.01) regions.

Broader regions of similar signed (but weaker) trend are also apparent, e.g., the positive trend across much of the western half of East Antarctica (i.e., the Dronning Maud Land and Western Indian Ocean sectors), indicating a consistent fast ice response to environmental forcing over a large spatial scale.

## 3.3 Bathymetric controls on fast ice distribution

Analysis of the bathymetric distribution of fast ice provides fundamental knowledge on the formation mode of fast ice (i.e., iceberg-associated vs formation within embayments). Circumpolar fast ice persistence as a two-dimensional histogram, binned by bathymetric depth is given in Fig. 6. This analysis indicates that the weighted (by persistence) mean depth of fast ice persistence occurs at ∼403 m, in line with earlier estimates linking fast ice extent with grounded icebergs in East Antarctica (Massom et al., 2001). The 403 m bathymetric contour is shown on Figure 2 as a solid grey line. This isobath only bears visual resemblance to areas containing persistent fast ice for much of East Antarctica (20° W to 172° E) and the Ross Sea (172° E to 130° W), indicating regional variability in either the actual iceberg grounding depth or the reliance of fast ice on the stability provided by grounded icebergs. Fig. S3 shows persistence-weighted histograms of fast ice formation depth for the eight newly-defined fast ice regions. Remarkable variability is observed across the regions, with the weighted mean of modal bathymetric depth ranging from >420 m (four contiguous regions from the Eastern Indian Ocean to the Amundsen Sea) to as shallow as ∼

200 m (Bellingshausen Sea sector), confirming that the ~400 m isobath is useful as an indicator of fast ice propensity only for certain regions.
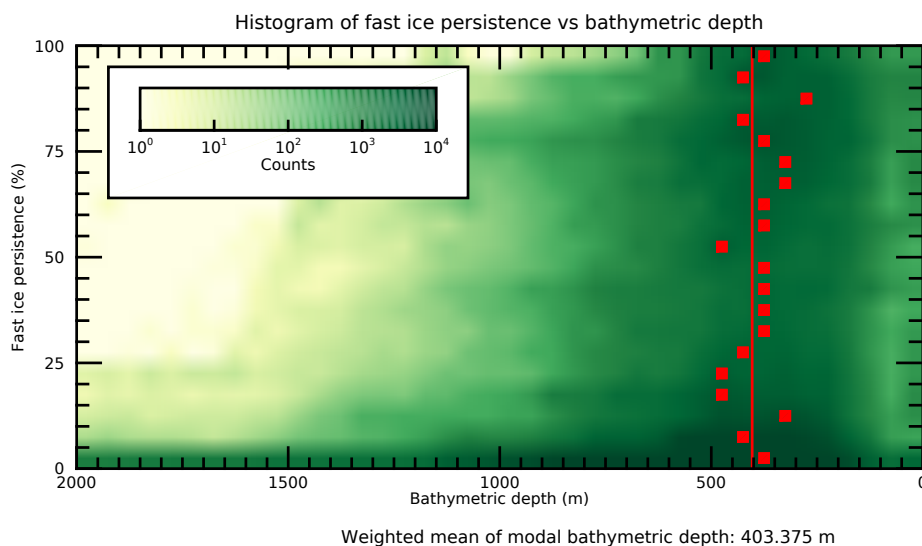
**Figure 6.** Two-dimensional histogram of circumpolar fast ice persistence (y-axis) versus bathymetryic depth (x-axis, taken from the International Bathymetryic Chart of the Southern Ocean (Arndt et al., 2013)). For each fast ice persistence bin (5% wide bins), the most frequent (modal) depth value is highlighted with a red square. The persistence-weighted mean of these modal values is indicated with the red vertical line, here corresponding to a bathymetryic depth of ~403 m.

## 4 Discussion

### 4.1 Fast ice distribution, age and trends

180 Overall, a significant and negative trend was found in circumpolar total sea ice extent (-882 $\pm$ 823 km$^2$/y or -0.19 $\pm$0.18 %/y, Fig. 5a). When partitioned into appropriate regions, opposing trends are observed in most neighbouring regions (Fig. 5b-i): positive trends in the Dronning Maud Land, Western Indian Ocean, Australia and Bellingshausen Sea regions; negative elsewhere. Fraser et al. Fraser et al. (2012) found that a significant positive trend was observed in the Indian Ocean sector (20 - 90° E) from March 2000 - Dec 2008. Here, we find that this trend, largely represented by the Western Indian Ocean region,

185 did not persist after 2008 (see Fig. 5b). Furthermore, persistent (e.g., 12 months or greater duration) "events" are evident in many anomaly plots (e.g., Fig. 5d, exhibiting a positive anomaly persisting from 2013 to 2014 in the Australia region, and contributing to the positive circumpolar total anomaly at the same time, Fig. 5a). Investigation of drivers of both regional trends and significant events within these regions is planned for the future. We note that the time series of circumpolar fast ice anomaly (Fig. 5a) bears close resemblance to that of overall sea ice extent (time series given in Fig. 2B of Parkinson (2019)),

190  with positive anomalies in 2007/08 and 2013/14, with a decline from 2014-2017. This association will also be explored more comprehensively in future work.

We find here an approximately threefold difference between maximum and minimum fast ice extent, with a minimum occurring in mid-March and a maximum in late September. The circumpolar seasonal cycle is much lower in amplitude that that of overall sea ice extent (with a wintertime maximum extent nearly six times higher than its summertime minimum, (Eayrs
195  et al., 2019; Parkinson, 2019)), a likely manifestation of the relatively large portion of fast ice which is multi-year combined with the limit of maximum fast ice extent imposed by the distribution of grounded icebergs.

## 4.2  Timing of maximum and minimum extent

The circumpolar fast ice cycle is delayed relative to that of overall sea ice, with the fast ice minimum (maximum) occurring 21 (nine) days later than the that of sea ice (shown in Table 1), in agreement with the findings of Fraser et al. (2012). In the
200  absence of particular case studies, which are out of scope here, we speculate that this lag may be due to one or more of the following reasons: a) adjacent pack ice may act as a protective buffer against dynamically-induced breakout (e.g., swell may be attenuated by adjacent pack, protecting the fast ice (Ushio, 2006)); b) the presence of pack ice at the fast ice edge may reduce "mode-3" summertime solar heating of the surface water (Jacobs et al., 1992), leading to lower basal melt rates under the fast ice (Arndt et al., 2020) and higher mechanical strength (Fedotov et al. (1998) estimate only 20-30% of wintertime flexural fast
205  ice strength remains by the time basal melt becomes widespread); or c) fast ice is simply able to persist longer into the summer due to the inherent shelter afforded by its formation within certain embayments (e.g., Lützow-Holm Bay, $\sim40°$ E, (Ushio, 2006)).

Regarding timing of maximum extent, Fraser et al. (2012) found that fast ice maximum occurs earlier than overall sea ice in the Indian Ocean and the Western Pacific Ocean sectors (covering much of East Antarctica). We find here that this result
210  holds for only three of eight newly-defined regions (Table 1), and that the timing in maximum extent is far more regionally variable (range: 48 d) than that of minimum extent (range: 13 d), a result also indicated spatially in Fig. 3. This is likely related to the bathymetric limit imposed on maximum fast ice extent, i.e., fast ice coverage around the outermost grounded icebergs is generally achieved by midwinter, and limited further growth occurs only upstream of obstacles to the coastal current, until September. Such growth is likely stochastic and event-based, imparting variability to the timing of maximum extent.

215  Based on a dataset covering the years 2006–2011 and 2016–2017, Li et al. (2020) found a mean November extent of $\sim$495,000 km$^2$, which is much lower than the mean maximum extent found here ($\sim$601,000 km$^2$). However, we have shown that November is after maximum fast ice extent in every region, so we suggest that circumpolar studies of maximum fast ice extent are best conducted around late September. Full consideration of the seasonality (i.e., timing of formation, breakout, and presence duration; and change in these quantities) of fast ice is outside of the scope of this paper, however complex regional
220  patterns have been identified in an analysis of overall East Antarctic sea ice seasonality (Massom et al., 2013), so future work on this is planned using the fast ice dataset (Fraser et al., 2020).

### 4.3 Bathymetric controls on fast ice distribution

We have shown large regional variability in the formation depth of fast ice, ranging from ∼200 m to ∼450 m (Fig. S3). Such regional variability has not been identified in earlier work (e.g., Massom et al., 2001; Fraser et al., 2012). This regional
225  dependence on bathymetry may also suggest fundamental regional differences in fast ice formation mode. As an example of this, consider the distribution of fast ice persistence by depth in the Bellingshausen Sea (Fig. S3, cyan line). In this region, relatively few grounded icebergs exist (Figure 4 in Li et al. (2020)), so fast ice predominantly forms between coastal margins (including islands), and is known as "regime 1" fast ice (Fraser et al., 2012). By contrast, in the Eastern Indian Ocean and Australia regions, "regime 2" fast ice predominates (Fraser et al., 2012), and a close relationship is found between grounded
230  icebergs and persistent fast ice (Li et al., 2020). In East Antarctica, icebergs have been observed to ground at depths up to around 400 m Massom (2003); Massom et al. (2009), although there is evidence for deeper grounding (in excess of 500 m) in some regions of the East Antarctic continental shelf (Beaman and Harris, 2005), and indeed newly-calved icebergs with keels of up to 600 m are known to calve from fast flowing outlet glaciers (Dowdeswell and Bamber, 2007). More detailed understanding of the mechanism of fast ice formation, as provided here, is crucial for development of the next generation of
235  prognostic regional fast ice models which require tuning of tensile strength (Lemieux et al., 2016).

### 4.4 Future work

Massom et al. (2010b) discussed a future scenario in which an increase in iceberg discharge from Antarctic ice shelves results in an increase in fast ice extent. In light of our analysis of fast ice persistence in the context of bathymetry, we suggest that this increase would occur only in those regions where few icebergs are currently available to ground on the shallow bathymetry,
240  i.e., the Bellingshausen Sea and Dronning Maud Land regions, as well as continental shelf shoals in the central Ross and Weddell seas (see 403 m bathymetric contour on Figure 2). Most other regions may already have sufficient density of grounded icebergs to act as fast ice anchors, as detailed in (Li et al., 2020). We also consider a future scenario in which the recently-detailed marine ice cliff instability mechanism is initiated (Pollard et al., 2015), whereby glacier/grounding line retreat results in high (>∼90 m) ice cliffs at the glacier terminus, resulting in calving of icebergs with extremely deep (in excess of 800 m)
245  keels. Evidence for this process exists in the form of very deep sediment scours around Pine Island Glacier (∼101 ° W, (Wise et al., 2017)), estimated to have occurred in the early Holocene. Presence of such deeply-keeled icebergs around the Antarctic continental shelf would allow the grounding of icebergs in new regions, completely altering the distribution of fast ice. For this reason, the next generation of coupled Antarctic ice/ocean models with fast ice should consider prognostic iceberg calving and grounding. Near-coastal bathymetric data paucity, leading to high uncertainty in current Antarctic bathymetric compilations, is
250  also a limiting factor for this kind of study, so should be addressed as a priority (Smith et al., in press). In addition to fields of smaller grounded bergs, it is also worth re-iterating the profound and unpredictable effects that large tabular icebergs can have on regional fast ice extent (e.g., Fogwill et al. (2016)), particularly when grounded for several decades.

    Compared to the earlier dataset covering only East Antarctica from 2000 to 2008 (Fraser et al., 2012), this new 18 y time series (Fraser et al., 2020) is a much more comprehensive dataset from which to gauge long-term change in fast ice extent.

255 However, we note that the more recent dataset is still shorter than the 30 y "climate" threshold defined by the World Meteo-
rological Organisation (Arguez and Vose, 2011). Indeed, the residence times of large grounded icebergs which have profound
effects on fast ice distribution can be as long as several decades (e.g., B09B which was grounded at ∼148 ° E from 1992 to
2010 (Leane and Maddison, 2018); A23A which has been grounded in the central Weddell Sea since 1991, i.e., currently 29
y (Paul et al., 2015)). As such, the 30 y threshold may also be appropriate to apply to Antarctic fast ice, in order to preclude
260 undue influence of stochastic large iceberg grounding, giving a strong impetus to extend this dataset.

Although our fast ice analysis is circum-Antarctic in extent, performed at a high spatio-temporal resolution and covers 18
y, it is still only limited to extent/distribution. The underlying dataset (Fraser et al., 2020) does not consider other physical
fast ice properties, including freeboard/thickness, thickness of overlying snow, roughness or albedo. Complete physical char-
acterisation of fast ice requires such data. Giles et al. (2008), working with synthetic aperture radar (SAR) imagery of East
265 Antarctic fast ice, indicated that thickness and roughness are likely closely related, ascribing values of 1.7 and 5.0 m thickness
to "smooth" and "rough" fast ice, respectively, however this is an overly-simplistic methodology for estimating thickness. Work
is underway on addressing this knowledge gap by remotely sensing circum-Antarctic fast ice roughness and thickness from
altimetric satellite data.

## 5   Conclusions

270 Here, using a newly-released, long-term (18 y), high-quality and high-resolution dataset of circum-Antarctic fast ice, we have
for the first time:

- – Presented the baseline characterisation of fast ice mean persistence, annual cycle, mean age, and timing of minimum and
  maximum extent;

- – Defined eight new fast ice regions based on fast ice anomaly co-variability;

275 - – Determined and discussed fast ice extent trends in these eight regions, revealing marked regional variability in trend (as
  well as inter-annual variability in fast ice extent within each region); and

- – Discussed fast ice characteristics in terms of its links with bathymetric depth, indicating formation modes within each
  region.

Although this work greatly advances the state of knowledge on Antarctic fast ice distribution and variability, deeper under-
280 standing of Antarctic fast ice is still limited by a paucity of studies on the environmental factors driving changes in fast ice
extent. One-dimensional thermodynamic studies have indicated the sensitivity of fast ice to environmental drivers, including
both the atmosphere and the ocean (e.g., Heil, 2006; Lei et al., 2010; Hoppmann et al., 2015; Brett et al., 2020), however
drivers of change in horizontal fast ice distribution are relatively poorly understood. Of the limited studies of fast ice extent for-
mation/breakout, a wide range of potential drivers have been identified (including remote atmospheric teleconnections (Aoki,
285 2017), a range of local atmospheric parameters (Fraser, 2011; Zhai et al., 2019; Leonard et al., 2021), swell-induced breakup

and anomalous snow cover (Ushio, 2006) and basal melt (Arndt et al., 2020)), however no unifying picture has emerged. Work is planned to use the new circumpolar fast ice dataset (Fraser et al., 2020) in conjunction with datasets of atmospheric and oceanic parameters to address this shortcoming, in order to elucidate such drivers. Due to regionally-specific drivers, we suggest that coupled ocean/sea ice models capable of realistically forming Antarctic fast ice are an important tool for studing fast

290 ice variability, and urgently need to be developed.

*Data availability.* The fast ice dataset analysed here is freely available at http://dx.doi.org/doi:10.26179/5d267d1ceb60c

## Appendix A: Sectoral anomalies and trends

In the main text, we focus on fast ice characteristics in newly-defined regions, as defined in the following section. Here, however we report the fast ice extent anomaly (observation minus repeated climatological cycle) and linear trend for the five commonly-

295 used oceanic sectors (Zwally et al., 1983), in order to assess their suitability for partitioning fast ice. These are shown in Fig. A1. Two sectors show significant trends: the Ross Sea (-1.43 ± 0.26 %/y) and the Bellingshausen and Amundsen seas sectors (0.67 ± 0.55 %/y). The remainder are insignificant, which may either be genuine features, or may indicate inappropriate (for fast ice) region selection (i.e., regions defined in this way may split areas of fast ice which co-vary).

## Appendix B: Selection of new regions

300 To investigate a more appropriate regional split, we perform cross-correlation on 1/4° longitude fast ice extent anomaly time-series (Fig. B1). Regions which co-vary exhibit high cross-correlation. Investigation of the fast ice anomaly cross-correlation matrix as a function of longitude indicates that eight regions are needed to appropriately partition fast ice, indicated as blue boxes.

Although this fundamental new region definition is based on a simple and robust methodology, its implementation and the

305 resulting regional definition in Antarctica require discussion. Firstly, since it is based on the cross-correlation of longitudinal slices, it is unable to separate distinct fast ice areas which share a longitude but differ in latitude. Such cases are encountered around a) 163 - 171° E (Victoria and Oates Land coasts); and b) 60 - 61° W (the eastern side of the Antarctic Peninsula). Although our technique is too simple to account for this longitudinal degeneracy, we note that in both cases, similar trends (Fig. 3b in the main text) are encountered at both areas of fast ice within the longitude zone (i.e., weak negative in the former,

310 and positive in the latter), giving confidence that the region definition is unaffected by this caveat.

Our region selection methodology indicates that the fast ice on the eastern side of the Antarctic Peninsula should be considered a part of the Bellingshausen Sea sector, rather than the Weddell Sea sector. This is somewhat surprising given the oceanic connection from this region to the rest of the Weddell Sea. However, this ice is much more proximal to the western side of the Antarctic Peninsula than it is to the fast ice in the eastern flank of the Weddell Sea region, indicating that localised
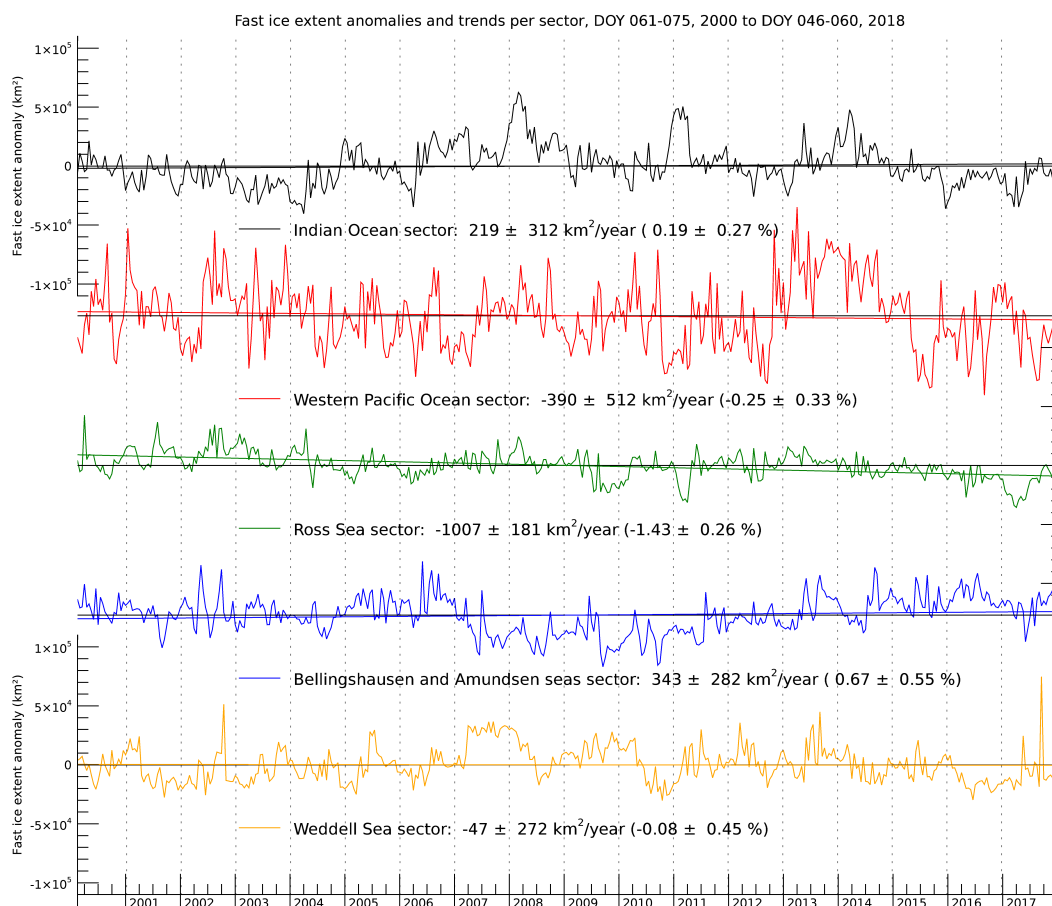
**Figure A1.** Fast ice extent anomaly time series for the 18 y period. Only the Bellingshausen and Amundsen seas and Ross Sea sectors show significant trends.

315   atmospheric conditions may be a dominant driver here. This hypothesis is supported by the positive fast ice trend encountered in the Bellingshausen Sea region – a region which has experienced a trend toward cooler surface air temperatures since the late 1990s (Turner et al., 2016).

    We also consider that the boundary between the Australia and Victoria and Oates Lands regions (at 146° E) may be an artefact of the "ice-scape" regime shift which occurred in the region after the ungrounding of iceberg B09B and subsequent

320   calving of the Mertz Glacier Tongue in 2010 (Leane and Maddison, 2018). To determine the influence of this event, the regional selection algorithm was re-run using only pre-calving post-calving fast ice anomaly data, with the result that the boundary location is correctly located in the pre-calving regime, but the fast ice variability off the Adélie/George V Land coast becomes somewhat more homogeneous in the post-calving regime, as expected following the removal of a major dynamical barrier, with the apparent regime boundary shifting to ∼160° E (not shown).
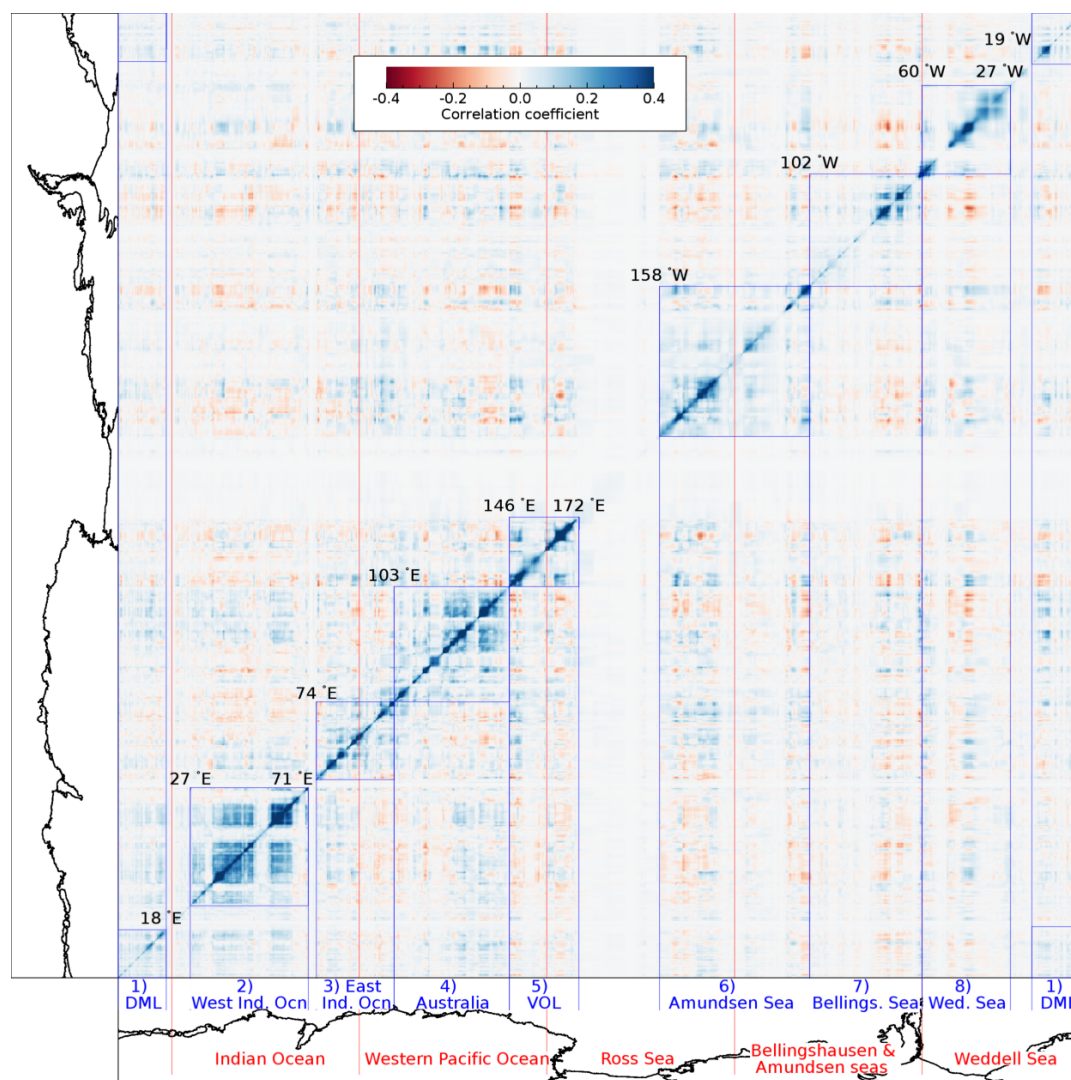
**Figure B1.** Fast ice anomaly cross-correlation matrix. Red vertical lines indicate the traditional sea ice sectors. Blue vertical lines and blue-outlined boxes highlight newly-defined pockets of high cross-correlation, indicating regions which co-vary.

## Appendix C: Regional bathymetric constraints on fast ice formation

In addition to the two dimensional histogram of fast ice persistence by bathymetric depth presented in the main text, we present in Fig C1 the projection of this two dimensional histogram onto the x-axis, linearly weighted by persistence (so that high-persistence fast ice contributes more). We also present this histogram for each newly-defined fast ice region (colored lines).
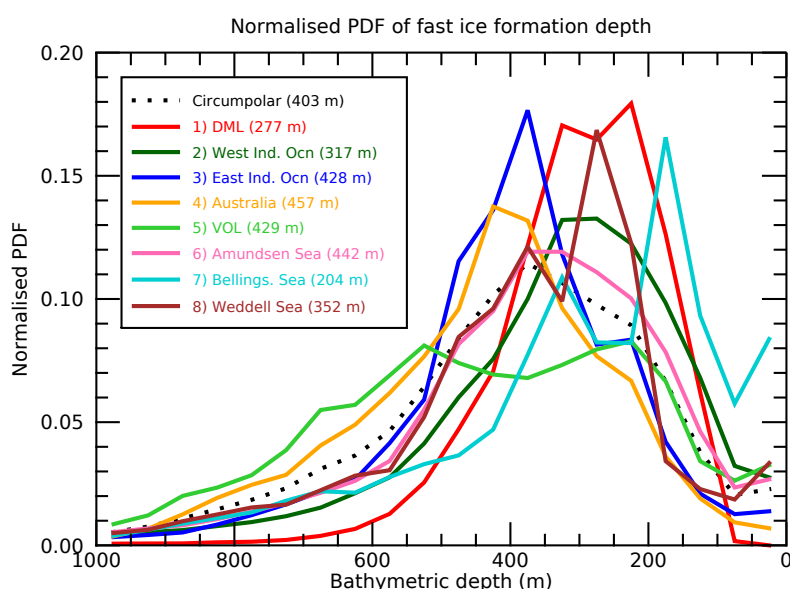
**Figure C1.** Normalised histograms of persistence-weighted fast ice formation depth for the eight newly-defined regions. Mean formation depth for each region is indicated in the legend.

*Author contributions.* All authors edited the manuscript. ADF led the analysis, produced all figures, drafted the paper and coordinated co-authors. RAM and KIO provided scientific and editorial feedback, and direction to the project. MSH and MNR provided statistical expertise in the time series analysis. ARK, ZW, PR, JC and RP-S assisted with data analysis, interpretation and visualisation.

*Competing interests.* The authors declare no competing interests.

*Acknowledgements.* This project received grant funding from the Australian Government as part of the Antarctic Science Collaboration
Initiative program, and contributes to Project 6 of the Australian Antarctic Program Partnership. This work was supported by the Australian
Research Council's Special Research Initiative for Antarctic Gateway Partnership (Project ID SR140300001), and contributes to Australian
Antarctic Science Project 4116. ADF is grateful to Chad Greene for discussions involving data presentation.

# References

Aoki, S.: Breakup of landfast sea ice in Lützow-Holm Bay, East Antarctica, and its teleconnection to tropical Pacific sea surface temperatures,
340    Geophysical Research Letters, 44, 3219 – 3227, 2017.

Arguez, A. and Vose, R. S.: The Definition of the Standard WMO Climate Normal: The Key to Deriving Alternative Climate Normals,
Bulletin of the American Meteorological Society, 92, 699 – 704, https://doi.org/10.1175/2010BAMS2955.1, 2011.

Arndt, J. E., Schenke, H. W., Jakobsson, M., Nitsche, F. O., Buys, G., Goleby, B., Rebesco, M., Bohoyo, F., Hong, J., Black, J., Greku, R.,
Udintsev, G., Barrios, F., Reynoso-Peralta, W., Taisei, M., and Wigley, R.: The International Bathymetric Chart of the Southern Ocean
345    (IBCSO) Version 1.0 - A new bathymetric compilation covering circum-Antarctic waters, Geophysical Research Letters, 40, 3111–3117,
https://doi.org/10.1002/grl.50413, 2013.

Arndt, S., Hoppmann, M., Schmithüsen, H., Fraser, A. D., and Nicolaus, M.: Seasonal and interannual variability of landfast sea ice in Atka
Bay, Weddell Sea, Antarctica, The Cryosphere, 14, 2775–2793, https://doi.org/10.5194/tc-14-2775-2020, 2020.

Beaman, R. J. and Harris, P. T.: Bioregionalisation of the George V Shelf, East Antarctica, Continental Shelf Research, 25, 1657–1691, 2005.

350    Brett, G. M., Irvin, A., Rack, W., Haas, C., Langhorne, P. J., and Leonard, G. H.: Variability in the distribution of fast
ice and the sub-ice platelet layer near McMurdo Ice Shelf, Journal of Geophysical Research: Oceans, 125, e2019JC015 678,
https://doi.org/https://doi.org/10.1029/2019JC015678, e2019JC015678 2019JC015678, 2020.

Clark, G. F., Stark, J. S., Palmer, A. S., Riddle, M. J., and Johnston, E. L.: The Roles of Sea-Ice, Light and Sedimentation in Structuring
Shallow Antarctic Benthic Communities, PLOS ONE, 12, 1–20, https://doi.org/10.1371/journal.pone.0168391, 2017.

355    de Jong, J., Schoemann, V., Maricq, N., Mattielli, N., Langhorne, P., Haskell, T., and Tison, J.-L.: Iron in land-fast sea ice of McMurdo
Sound derived from sediment resuspension and wind-blown dust attributes to primary productivity in the Ross Sea, Antarctica, Marine
Chemistry, 157, 24 – 40, https://doi.org/https://doi.org/10.1016/j.marchem.2013.07.001, 2013.

Dowdeswell, J. and Bamber, J.: Keel depths of modern Antarctic icebergs and implications for sea-floor scouring in the geological record,
Marine Geology, 243, 120 – 131, https://doi.org/https://doi.org/10.1016/j.margeo.2007.04.008, 2007.

360    Eayrs, C., Holland, D., Francis, D., Wagner, T., Kumar, R., and Li, X.: Understanding the Seasonal Cycle of Antarctic Sea Ice Extent in
the Context of Longer-Term Variability, Reviews of Geophysics, 57, 1037–1064, https://doi.org/https://doi.org/10.1029/2018RG000631,
2019.

Fedotov, V. I., Cherepanov, N. V., and Tyshko, K. P.: Some features of the growth, structure and metamorphism of East Antarctic landfast
sea ice, Antarctic Sea Ice: Physical Processes, Interactions and Variability, Antarctic Research Series, 74, 343–254, 1998.

365    Fogwill, C. J., van Sebille, E., Cougnon, E. A., Turney, C. S. M., Rintoul, S. R., Galton-Fenzi, B. K., Clark, G. F., Marzinelli, E. M.,
Rainsley, E. B., and Carter, L.: Brief communication: Impacts of a developing polynya off Commonwealth Bay, East Antarctica, triggered
by grounding of iceberg B09B, The Cryosphere, 10, 2603–2609, https://doi.org/10.5194/tc-10-2603-2016, 2016.

Fraser, A. D.: East Antarctic Landfast Sea Ice Distribution and Variability, Ph.D. thesis, University of Tasmania, 2011.

Fraser, A. D., Massom, R. A., and Michael, K. J.: A Method for Compositing Polar MODIS Satellite Images to Re-
370    move Cloud Cover for Landfast Sea-Ice Detection, IEEE Transactions on Geoscience and Remote Sensing, 47, 3272–3282,
https://doi.org/10.1109/TGRS.2009.2019726, 2009.

Fraser, A. D., Massom, R. A., and Michael, K. J.: Generation of high-resolution East Antarctic landfast sea-ice maps from cloud-free MODIS
satellite composite imagery, Remote Sensing of Environment, 114, 2888–2896, https://doi.org/10.1016/j.rse.2010.07.006, 2010.

Fraser, A. D., Massom, R. A., Michael, K. J., Galton-Fenzi, B. K., and Lieser, J. L.: East Antarctic Landfast Sea Ice Distribution and

375    Variability, 2000-08, Journal of Climate, 25, 1137–1156, https://doi.org/10.1175/JCLI-D-10-05032.1, 2012.

Fraser, A. D., Ohshima, K. I., Nihashi, S., Massom, R. A., Tamura, T., Nakata, K., Williams, G. D., Carpentier, S., and Willmes, S.: Landfast ice controls on sea-ice production in the Cape Darnley Polynya: A case study, Remote Sensing of Environment, 233, https://doi.org/https://doi.org/10.1016/j.rse.2019.111315, 2019.

Fraser, A. D., Massom, R. A., Ohshima, K. I., Willmes, S., Kappes, P. J., Cartwright, J., and Porter-Smith, R.: High-resolution mapping of

380    circum-Antarctic landfast sea ice distribution, 2000–2018, Earth System Science Data, 2020, 2987–2999, https://doi.org/10.5194/essd-2020-99, 2020.

Giles, A. B., Massom, R. A., and Lytle, V. I.: Fast-ice distribution in East Antarctica during 1997 and 1999 determined using RADARSAT data, Journal of Geophysical Research (Oceans), 113, https://doi.org/10.1029/2007JC004139, 2008.

Greene, C. A., Young, D. A., Gwyther, D. E., Galton-Fenzi, B. K., and Blankenship, D. D.: Seasonal dynamics of Totten Ice Shelf controlled

385    by sea ice buttressing, The Cryosphere, 12, 2869–2882, https://doi.org/10.5194/tc-12-2869-2018, 2018.

Handcock, M. S. and Raphael, M. N.: Modeling the annual cycle of daily Antarctic sea ice extent, The Cryosphere, 14, 2159–2172, https://doi.org/10.5194/tc-14-2159-2020, 2020.

Heil, P.: Atmospheric conditions and fast ice at Davis, East Antarctica: A case study, Journal of Geophysical Research (Oceans), 111, 5009–5023, 2006.

390  Hoppmann, M., Nicolaus, M., Hunkeler, P. A., Heil, P., Behrens, L.-K., König-Langlo, G., and Gerdes, R.: Seasonal evolution of an ice-shelf influenced fast-ice regime, derived from an autonomous thermistor chain, Journal of Geophysical Research: Oceans, 120, 1703–1724, https://doi.org/https://doi.org/10.1002/2014JC010327, 2015.

Jacobs, S., Helmer, H., Doake, C. S. M., Jenkins, A., and Frolich, R. M.: Melting of ice shelves and the mass balance of Antarctica, Journal of Glaciology, 38, 375–387, https://doi.org/10.3189/S0022143000002252, 1992.

395  Kim, M., Han, H., Im, J., Lee, S., and Kim, H.-C.: Object-based Landfast Sea Ice Detection Over West Antarctica Using Time Series of ALOS PALSAR Data, Remote Sensing of Environment, 242, 2020.

Kim, S., Saenz, B., Scanniello, J., Daly, K., and Ainley, D.: Local climatology of fast ice in McMurdo Sound, Antarctica, Antarctic Science, 30, 125–142, https://doi.org/10.1017/S0954102017000578, 2018.

Kooyman, G. L. and Burns, J.: Weddell seal versus Emperor penguin: Boss of the Ross Sea, American Zoology, 39, 9–19, 1999.

400  Kusahara, K., Hasumi, H., Fraser, A. D., Aoki, S., Shimada, K., Williams, G. D., Massom, R., and Tamura, T.: Modeling Ocean-Cryosphere Interactions off Adélie and George V Land, East Antarctica, Journal of Climate, 30, 163–188, https://doi.org/10.1175/JCLI-D-15-0808.1, 2017.

Leane, E. and Maddison, B.: A biography of iceberg B09B, Australian Humanities Review, 63, 99 – 115, 2018.

Lei, R., Li, Z., Cheng, B., Zhang, Z., and Heil, P.: Annual cycle of landfast sea ice in Prydz Bay, east Antarctica, Journal of Geophysical

405  Research (Oceans), 115, 2006, https://doi.org/10.1029/2008JC005223, 2010.

Lemieux, J.-F., Dupont, F., Blain, P., Roy, F., Smith, G. C., and Flato, G. M.: Improving the simulation of landfast ice by combining tensile strength and a parameterization for grounded ridges, Journal of Geophysical Research: Oceans, 121, 7354–7368, https://doi.org/https://doi.org/10.1002/2016JC012006, 2016.

Leonard, G. H., Turner, K. E., Richter, M. E., Whittaker, M. S., and Smith, I. J.: Brief communication: The anomalous winter 2019 sea ice

410  conditions in McMurdo Sound, Antarctica, The Cryosphere Discussions, 2021, 1–10, https://doi.org/10.5194/tc-2020-352, 2021.

Li, X., Shokr, M., Hui, F., Chi, Z., Heil, P., Chen, Z., Yu, Y., Zhai, M., and Cheng, X.: The spatio-temporal patterns of landfast ice in Antarctica during 2006-2011 and 2016-2017 using high-resolution SAR imagery, Remote Sensing of Environment, 242, 111 736, https://doi.org/https://doi.org/10.1016/j.rse.2020.111736, 2020.

Markwardt, C. B.: Non-linear Least-squares Fitting in IDL with MPFIT, in: Astronomical Data Analysis Software and Systems XVIII, edited by D. A. Bohlender, D. Durand, & P. Dowler, vol. 411 of *Astronomical Society of the Pacific Conference Series*, p. 251, 2009.

Massom, R., Reid, P., Stammerjohn, S., Raymond, B., Fraser, A. D., and Ushio, S.: Change and Variability in East Antarctic Sea Ice Seasonality, 1979/80–2009/10, PLOS ONE, 2013.

Massom, R. A.: Recent iceberg calving events in the Ninnis Glacier region, East Antarctica, Antarctic Science, 15 (2), 303–313, 2003.

Massom, R. A., Harris, P. T., Michael, K. J., and Potter, M. J.: The distribution and formative processes of latent-heat polynyas in East Antarctica, Annals of Glaciology, 27, 420–426, 1998.

Massom, R. A., Hill, K. L., Lytle, V. I., Worby, A. P., Paget, M. J., and Allison, I.: Effects of regional fast-ice and iceberg distributions on the behaviour of the Mertz Glacier Polynya, East Antarctica, Annals of Glaciology, 33, 391–398, 2001.

Massom, R. A., Hill, K., Barbraud, C., Adams, N., Ancel, A., Emmerson, L., and Pook, M.: Fast ice distribution in Adélie Land, East Antarctica: Interannual variability and implications for Emperor penguins (*Aptenodytes forsteri*), Marine Ecology Progress Series, 374, 243–257, 2009.

Massom, R. A., Giles, A. B., Fricker, H. A., Warner, R., Legrésy, B., Hyland, G., Young, N., and Fraser, A. D.: Examining the interaction between multi-year landfast sea ice and the Mertz Glacier Tongue, East Antarctica; Another factor in ice sheet stability?, Journal of Geophysical Research (Oceans), 115, C12 027, https://doi.org/10.1029/2009JC006083, 2010a.

Massom, R. A., Reid, P., Stammerjohn, S., and Barreira, S.: Antarctica: Sea ice extent and concentration, in: State of The Climate in 2008, edited by Arndt, D. S., Baringer, M. O., and Johnson, M. R., vol. 91, pp. S131–S133, Bulletin of the American Meteorological Society, 2010b.

Massom, R. A., Giles, A. B., Warner, R. C., Fricker, H. A., Legrésy, B., Hyland, G., Lescarmontier, L., and Young, N.: External influences on the Mertz Glacier Tongue (East Antarctica) in the decade leading up to its calving in 2010, Journal of Geophysical Research: Earth Surface, 120, 490–506, https://doi.org/10.1002/2014JF003223, 2015.

Massom, R. A., Scambos, T. A., Bennetts, L. G., Reid, P., Squire, V. A., and Stammerjohn, S. E.: Antarctic ice shelf disintegration triggered by sea ice loss and ocean swell, Nature, 558, 383 – 389, https://doi.org/https://doi.org/10.1038/s41586-018-0212-1, 2018.

Meiners, K. M., Vancoppenolle, M., Carnat, G., Castellani, G., Delille, B., Delille, D., Dieckmann, G. S., Flores, H., Fripiat, F., Grotti, M., Lange, B. A., Lannuzel, D., Martin, A., McMinn, A., Nomura, D., Peeken, I., Rivaro, P., Ryan, K. G., Stefels, J., Swadling, K. M., Thomas, D. N., Tison, J.-L., van der Merwe, P., van Leeuwe, M. A., Weldrick, C., and Yang, E. J.: Chlorophyll-a in Antarctic Landfast Sea Ice: A First Synthesis of Historical Ice Core Data, Journal of Geophysical Research: Oceans, 123, 8444–8459, https://doi.org/10.1029/2018JC014245, 2018.

Meredith, M., Sommerkorn, M., Cassotta, S., Derksen, C., Ekaykin, A., Hollowed, A., Kofinas, G., Mackintosh, A., Melbourne-Thomas, J., Muelbert, M. M. C., Ottersen, G., Pritchard, H., and Schuur, E. A. G.: IPCC Special Report on the Ocean and Cryosphere in a Changing Climate, chap. Polar Regions, p. 215, Cambridge University Press, Cambridge, 2019.

Nihashi, S. and Ohshima, K. I.: Circumpolar mapping of Antarctic coastal polynyas and landfast sea ice: Relationship and variability, Journal of Climate, 28, 3650–3670, 2015.

Ohshima, K. I., Fukamachi, Y., Williams, G. D., Nihashi, S., Roquet, F., Kitade, Y., Tamura, T., Hirano, D., Herraiz-Borreguero, L., Field, I., Hindell, M., Aoki, S., and Wakatsuchi, M.: Antarctic Bottom Water production by intense sea-ice formation in the Cape Darnley polynya, Nature Geoscience, 6, 235–240, https://doi.org/10.1038/ngeo1738, 2013.

450 Parkinson, C. L.: A 40-y record reveals gradual Antarctic sea ice increase followed by decreases at rates far exceeding the rates seen in the Arctic, Proceedings of the National Academy of Sciences, 2019.

Paul, S., Willmes, S., and Heinemann, G.: Long-term coastal-polynya dynamics in the southern Weddell Sea from MODIS thermal-infrared imagery, The Cryosphere, 9, 2027–2041, https://doi.org/10.5194/tc-9-2027-2015, 2015.

Pollard, D., DeConto, R. M., and Alley, R. B.: Potential Antarctic Ice Sheet retreat driven by hydrofracturing and ice cliff failure, Earth and
455 Planetary Science Letters, 412, 112 – 121, 2015.

Raphael, M. N. and Hobbs, W.: The influence of the large-scale atmospheric circulation on Antarctic sea ice during ice advance and retreat seasons, Geophysical Research Letters, 41, 5037–5045, https://doi.org/https://doi.org/10.1002/2014GL060365, 2014.

Shadwick, E., Rintoul, S., Tilbrook, B., Williams, G., Young, N., D. Fraser, A., Marchant, H., Smith, J., and Tamura, T.: Glacier tongue calving reduced dense water formation and enhanced carbon uptake, Geophysical Research Letters, 40, 904–909,
460 https://doi.org/10.1002/grl.50178, 2013.

Smith, J., Nogi, Y., Spinoccia, M., Dorschel, B., and Leventer, A.: A new bathymetric compilation of the Cape Darnley region, East Antarctica, Antarctic Science, in press.

The Council of Managers of National Antarctic Programs (COMNAP), ed.: COMNAP Sea Ice Challenges Workshop proceedings, vol. ISBN 978-0-473-34368-2, COMNAP, COMNAP Secretariat, Christchurch, New Zealand, https://www.comnap.aq/documents/COMNAP_Sea_
465 Ice_Challenges_BKLT_Web_Final_Dec2015.pdf, 2015.

Turner, J., Lu, H., White, I., King, J. C., Phillips, T., Hosking, J. S., Bracegirdle, T. J., Marshall, G. J., Mulvaney, R., and Deb, P.: Absence of 21st century warming on Antarctic Peninsula consistent with natural variability, Nature, 2016.

Ushio, S.: Factors affecting fast-ice break-up frequency in Lützow-Holm Bay, Antarctica, Annals of Glaciology, 44, 177–182, 2006.

Vaughan, D. G., Comiso, J. C., Allison, I., Carrasco, J., Kaser, G., Kwok, R., Mote, P., Murray, T., Paul, F., Ren, J., Rignot, E., Solomina,
470 O., Steffen, K., and Zhang, T.: Climate Change 2013: The Physical Science Basis. Contribution of Working Group I to the Fifth Assessment Resport of the Intergovernmental Panel on Climate Change, chap. Observations: Cryosphere, p. 334, Cambridge University Press, Cambridge, 2013.

Wise, M., Dowdeswell, J., and Jakobsson, M.: Evidence of marine ice-cliff instability in Pine Island Bay from iceberg-keel plough marks, Nature, 550, 506–510, 2017.

475 World Meteorological Organization: WMO sea-ice nomenclature. Terminology, codes and illustrated glossary, Tech. Rep. 259, Geneva Secretariat of the World Meterological Organization, 1970.

Zhai, M., Zhao, T., Hui, F., Cheng, X., Liu, A., Yuan, J., Yu, Y., and Ding, Y.: Anomalous extensive landfast sea ice in the vicinity of Inexpressible Island, Antarctica, Advances in Polar Science, 30, 406 – 411, 2019.

Zwally, H. J., Comiso, J. C., Parkinson, C. L., Campbell, W. J., Carsey, F. D., and Gloersen, P.: Antarctic Sea Ice, 1973-1976: Satellite
480 Passive-Microwave Observations. NASA SP-459, NASA Special Publication, 459, 1983.